Journal Name

ARTICLE

Influence of geometric isomerism on the binding of platinum anticancer agents with phospholipids

Anil Kumar Gorle,[‡a] Junyong Zhang, [‡¶b] Susan J. Berners-Price*[ab] and Nicholas P. Farrell*[ca]

Received 00th January 20xx,
Accepted 00th January 20xx

DOI: 10.1039/x0xx00000x

www.rsc.org/

Reported herein is a detailed NMR and DFT study of the interaction of the ^{15}N-labelled dinuclear platinum anticancer compound [{*cis*-PtCl(NH_3)$_2$}$_2${μ-$H_2N(CH_2)_6NH_2$}]$^{2+}$ (^{15}N-**1**, 1,1/*c,c*) with 1,2-dihexanoyl-*sn*-glycero-3-phosphate (DHPA), as a comparison with an earlier study of the interaction of the same water-soluble phospholipid fragment with the geometric *trans* isomer (1,1/*t,t*). The reaction of ^{15}N-**1** with the sodium salt of DHPA was studied at 298 K, pH ~5.6, by [^{1}H,^{15}N] HSQC 2D NMR spectroscopy. The NMR data, supported by DFT models, provide evidence that the monofunctional DHPA adduct of ^{15}N-**1** exists in two conformational forms, with different orientation of the $(CH_2)_6$ linker; one has an interaction between the unbound {PtN_3Cl} moiety and the coordinated DHPA molecule. Similarly, two bifunctional adduct conformers are identified, in which one has an interaction between the phosphate groups of the two bound DHPA molecules. When compared to the previously reported reactions of 1,1/*t,t* with DHPA, equilibrium conditions of the 1,1/*c,c* reaction are reached more slowly (120 h), similar to the reaction with phosphate. The rate constant for the first step of DHPA binding (k_L) is slightly lower (1.6 fold) for the *cis*- compared to the *trans*-isomer, whereas the rate constants for the reverse reaction is 4-fold lower, resulting in a much greater proportion of DHPA bound species at equilibrium.

Introduction

Platinum chemistry has been in the forefront of elucidation of kinetics and mechanisms of substitution reactions in inorganic chemistry.[1] The favourable kinetic profiles (reactions with half-lives of hours and days) were perhaps very well suited for an era with less advanced technical instrumentation than exists today and most textbooks rely heavily on examples of platinum complex reactions to elucidate the principles of associative reactions and elaborate on theoretical and practical aspects of the kinetic *trans* effect as well as the thermodynamic *trans* influence. Dominating and underpinning many of these aspects is the concept of Pt(II) as a quintessential 'soft' acid with high affinity for soft bases such as sulphur nucleophiles. Nitrogen donors, especially of "aromatic" systems such as pyridine or delocalised systems of purines and pyrimidines can be considered as intermediate soft bases. This balance is manifested in many discussions of the biological activity of platinum complexes – comparing metabolism and deactivation (predominantly S-binding) and target activation/fixation (Pt-N binding on DNA). In either case, covalent binding is expected to produce essentially irreversible reactions with formation of strong Pt-S and Pt-N bonds. In contrast, systematic study of oxygen donors in biology is lacking, especially with respect to formation of Pt-O-donor species in reaction pathways associated with perhaps substitution-labile or transient species formed during metabolism, cell entry and even target binding. Monodentate O-donors are hard bases and Pt-O bonds are expected to be more substitution-labile compared to chloride, or N and S-donors (HSAB). Nevertheless, these interactions could be relevant in the biological milieu due to high local concentrations of common "weak" ligands such as carbonate and sulfate.

In previous work we pioneered the use of [^{1}H,^{15}N] NMR spectroscopy to explore the aquation chemistry of cisplatin[2] and other platinum anticancer complexes[3] including polynuclear platinum complexes (PPCs).[4, 5] We have also carried out detailed studies exploring the kinetics of binding of PPCs to simple O-donor anions (phosphate, acetate and sulfate)[6, 7] and showed how subtle changes to the platinum coordination sphere (*trans* vs *cis* isomers) influences the pK_a of the coordinated aqua ligands and the speciation profile.[6]

In recent work we have built on these fundamental studies to explore the binding of PPCs to neglected biological targets with O-donor ligands: Heparan Sulfate Proteoglycans (HSPGs) and phospholipids, which are important components of cell membranes and are involved in PPC cellular internalization.[8] Our studies focus on developing a detailed understanding of reactions with simple model complexes, which can then be extrapolated to relevant biological targets. For example, we have investigated the interaction of the trinuclear (Triplatin or 1,0,1/*t,t,t*) and dinuclear (1,1/*t,t*) PPCs with three D-glucosamine residues containing varied O-sulfate and N-sulfate or N-acetyl substitutions, which represent monosaccharide fragments present within the repeating disaccharide sequences of cell surface heparan sulfate.[9] We have studied also the interaction of these PPCs with 1,2-dihexanoyl-*sn*-glycero-3-phosphate (DHPA), a

[a] *Institute for Glycomics, Griffith University, Gold Coast Campus, Southport, Queensland, 4222, Australia. Email: s.berners-price@griffith.edu.au.*
[b] *School of Biomedical, Biomolecular & Chemical Sciences, University of Western Australia, Crawley, WA, 6009, Australia.*
[c] *Department of Chemistry, Virginia Commonwealth University, Richmond, 23284, Virginia, USA. Email: npfarrell@vcu.edu.*
†Electronic Supplementary Information (ESI) available: Scientist equation files. See DOI: 10.1039/x0xx00000x
‡ These authors contributed equally to the manuscript
¶ Present address: College of Biological, Chemical Science and Engineering, Jiaxing University, Jiaxing University, Jiaxing 314001, P.R. China.

shorter, water-soluble model for the phospholipid DPPA (Chart 1).[10] These latter studies showed that the monofunctional DHPA adduct of 1,1/*t,t* coordinated to a second DHPA molecule in two different orientations, leading to formation of two conformers of the bifunctional adduct. Triplatin, which contains a charged $\{PtN_4\}^{2+}$ central linker, is capable of forming higher order structures through "phosphate clamp" interactions with two molecules of DHPA.

In the present paper, we study the effect of geometric isomerism on phospholipid binding by comparing the previously studied dinuclear *trans* isomer (1,1/*t,t*) to its *cis* isomer (1,1/*c,c*). The kinetics of 1,1/*c,c*-DHPA binding are also compared with previous studies on simple phosphate binding and with those reported for the binding of 1,0,1/*t,t,t* and 1,1/*t,t* with DHPA.[10] The work highlights how the interplay of modern experimental ([^{1}H, ^{15}N] NMR spectroscopy) and theoretical (DFT modelling) techniques allows prediction of interactions of platinum anticancer complexes with relevant biological targets by extrapolating studies with simple model systems.

<Insert Chart 1 here>

Results and Discussion

NMR studies

The reaction of ^{15}N-**1** with DHPA (1:5 mol ratio) in 100 mM $NaClO_4$ reaction was followed for a period of 5 days in the approach to equilibrium. Representative [^{1}H,^{15}N] HSQC NMR spectra are shown in Fig. 1 and the chemical shifts of the species observed during the reaction are listed in Table 1. The assignment of the species observed was made based on the previous reaction of 1,1/*c,c* with phosphate[6] and comparison of the ^{1}H and ^{15}N chemical shifts of the peaks in the *cis*- and *trans*-NH_3 and Pt–NH_2 regions.

<Insert Figure 1 and Table 1 here>

In the first spectrum recorded after 36 min (Fig. 1(a)), in addition to the peaks for ^{15}N-**1** (labelled A), there are three peaks assignable to the $\{PtN_3O\}$ group of the monoaquated species (labelled B) with chemical shifts consistent with those obtained from pH titration curves at this pH (5.6).[6]

Monofunctional adduct formation. Careful inspection of the [^{1}H,^{15}N] HSQC NMR spectra provides evidence for two different conformational forms of the monofunctional DHPA adduct. ^{1}H,^{15}N peaks assignable to the first formed adduct (1,1/*c,c*-MF-1) were just visible in the first spectrum and continued to increase in intensity over time. In contrast to the reaction with phosphate,[6] in the *trans*-NH_3 region the peak for the $\{PtN_3Cl\}$ group (labelled $C_{m'}$, Fig. 1(b)) is slightly deshielded in the ^{1}H dimension ($\Delta\delta$ 0.03) and distinguishable from that of the parent chlorido species, suggesting an interaction with the bound DHPA molecule. Notably the *cis*-geometry allows interactions between the two end $\{PtN_3Y\}$ groups of 1,1/*c,c* that is not possible in the 1,1/*t,t* case.[6] A strongly deshielded peak at δ 4.61/–42.8 (labelled $C_{m'}$, Fig. 1(b)), is assigned to the Pt-NH_2 protons *cis* to the unbound chlorido group, on the basis of the H-bonding interactions observed in the model (Fig. 2(a), see below). In the second monofunctional adduct (1,1/*c,c*-MF-2) there is no interaction between the $\{PtN_3O\}$ and $\{PtN_3Cl\}$ groups (Fig, 2(b)) and hence the ^{1}H/^{15}N peaks for the $\{PtN_3Cl\}$ group will be coincident with that of the parent species.

For both adducts, coordination of the DHPA molecule by the phosphate O atom places the *cis*-NH_3 in a similar hydrogen bonded environment to that previously reported for the Pt-NH_3 groups in 1,1/*t,t*,[10] and this peak (δ 3.86/–65.3, labelled C_m) is similarly deshielded in both ^{1}H ($\Delta\delta = 0.10$) and ^{15}N ($\Delta\delta = 0.7$) dimensions with respect to the parent chlorido species. The Pt–NH_2 group (δ 4.56/–43.5), which is similarly *cis* to the coordinated DHPA molecule, exhibits a similar deshielding with respect to the parent chlorido complex (^{1}H $\Delta\delta = 0.07$, ^{15}N $\Delta\delta = 0.7$). The *trans*-NH_3 group (δ 4.21/–83.6) is noticeably shielded in the ^{1}H dimension ($\Delta\delta$ –0.08) with respect to the parent chlorido complex, whereas in the case of 1,1/*t,t* the ^{1}H shifts for the analogous Pt-NH_2 protons were almost identical in species A and C.[10]

By observing the change in intensity of *trans*-NH_3 peak for the unbound $\{PtN_3Cl\}$ group ($C_{m'}$ Fig. 1) the mono-DHPA adduct (1,1/*c,c*-MF-1) reached a maximum intensity after about 9 h, and then decreased so that it represents only 2% of the total Pt species at equilibrium

Bifunctional adduct formation. In the reaction of 1,1/*c,c* with phosphate,[6] distinct peaks were observed in the *trans*-NH_3 region assignable to the phosphatoaqua species, attributable to an interaction between the coordinated aqua and phosphato groups which influences the ^{1}H chemical shift of the *trans*-NH_3 ligand. This species is an intermediate to the formation of the macrochelate phosphate bridged species which represented 25% of the total Pt species at equilibrium. No similar peaks were observed in the reaction with DHPA indicating that there is no interaction between the bound DHPA phosphate group and the unbound $\{PtN_3OH_2\}$ moiety. However, analysis of the ^{1}H,^{5}N peaks, in conjunction with the DFT models (below), provides evidence for formation of two distinct bifunctional DHPA adducts. ^{1}H,^{15}N peaks assignable to 1,1/*c,c*-BF-1 (labelled D) were first visible after about 4 h and grow slowly accounting for 18% of the final total Pt species. There are significant changes in ^{1}H and ^{15}N shifts indicative of interactions between the two bound DHPA molecules. The protons of the *cis*-NH_3 and Pt–NH_2 groups (both *cis* to the bound DHPA molecule) are more strongly deshielded ($\Delta\delta$ 0.04 (NH_3) and 0.09 (NH_2)); the protons of the *trans*-NH_3 group are similarly deshielded ($\Delta\delta$ 0.05), whereas a shielding ($\Delta\delta$ –0.4) is observed in the ^{15}N dimension. For the second bifunctional adduct (1,1/*c,c*-BF-2), the ^{1}H and ^{15}N chemical shifts of the Pt-NH_2 and *cis*- and *trans*-NH_3 groups of the bound $\{PtN_3O\}$ groups (peaks labelled C_b in Figs. 1(b and c)) are indistinguishable from those in the mono-DHPA adduct(s) (C_m) indicating that there is no interaction between the two ends of the 1,1/*c,c* molecule. These peaks represent 64% of the total Pt species present at the end of the reaction.

DFT modelling

Two DFT optimized models for the monofunctional adduct of 1,1/*c,c* with DHPA were constructed and are shown in Fig. 2 (a and b).

<Insert Figure 2 here>

In the first model (1,1/*c,c*-MF-1; (Fig. 2(a)) the orientation of the $(CH_2)_6$ chain enables the unbound $\{PtN_3Cl\}$ sphere to interact with the coordinated DHPA molecule. The model is analogous to previously constructed models of 1,1/*c,c* aquation products in phosphate, where the *cis*-geometry enabled interaction between the two Pt coordination spheres.[6] Expansion of the H-bonding interactions are

shown in Fig. 3 (a and b). For the {PtN_3O} moiety (Fig. 3(a)) the *cis*-NH_3 group has short H-bonds to the $POCH_2$ oxygen atom (distance = 2.36 Å) and the carbonyl oxygen from DHPA aliphatic chain b (distance = 2.00 Å), which also has a H-bond (distance = 2.20 Å) to the *trans*-NH_3 group. There are no H-bonds involving the Pt–NH_2 protons. For the {PtN_3Cl} moiety (Fig. 3(b)) a hydrogen bond between the *trans*-NH_3 group and the carbonyl oxygen of chain a of the coordinated DHPA (distance = 2.05 Å), is consistent with the observation of a distinct $^1H/^{15}N$ peak ($C_{m'}$; Fig. 1(b)). The NH_2 group is H-bonded to both the same carbonyl oxygen (distance = 2.20 Å) and the phosphate oxygen of the coordinated DHPA (distance = 1.97 Å) and is consistent with the strongly deshielded $^1H,^{15}N$ peak in the Pt-NH_2 region ($C_{m'}$;Fig 1(b)).

For the second model (1,1/*c,c*-MF-2; Fig. 2(b)), the $(CH_2)_6$ chain has a similar elongated orientation to that in the 1,1/*t,t* adduct reported previously, so that there is no interaction between the two {PtN_3Y} coordination spheres and the am(m)ine protons form analogous H-bonds to the coordinated DHPA molecule (Fig. 4(a)).[10] The *cis*-NH_3 group has a short H-bond to the phosphate oxygen atom (distance = 1.95 Å), whilst the NH_2 group (analogous to one of the *cis*-NH_3 groups in 1,1/*t,t*) has a short H-bond (distance = 1.97 Å) to the carbonyl oxygen from DHPA aliphatic chain a. The *trans*-NH_3 group is analogous to the NH_2 group in 1,1/*t,t* and similarly is not involved in any H-bonding interaction. These features are consistent with the ^1H shifts in the [$^1H,^{15}N$] HSQC NMR spectra (Fig. 1) where peaks (C_m) in the *cis*-NH_3 and Pt–NH_2 regions are strongly deshielded, whereas the *trans*-NH_3 peak is slightly shielded compared to the parent chlorido species.

The NMR data provide evidence for different conformers of the bifunctional adduct in which there is either an interaction, or no interaction between the two {PtN_3O} groups. The DFT optimized model (1,1/*c,c*-BF-1) shown in Fig. 2(c) (and Fig. 3(c and d)) has a hydrogen bonding interaction between the phosphate groups of the two bound DHPA molecules and is consistent with the strongly deshielded Pt-am(m)ine protons (peaks D in Fig. 1(c)). The positioning of the two Pt coordination spheres in close proximity enables a short H-bond (distance = 1.85 Å) between one of the Pt–NH_2 groups and the phosphate oxygen of the DHPA coordinated to the other Pt atom, and a second H-bond (distance = 2.08 Å) to the carbonyl oxygen on aliphatic chain a of the coordinated DHPA. The second NH_2 group has a single H-bond (distance = 2.44 Å) to the $POCH_2$ oxygen atom of the coordinated DHPA molecule. Both *trans*-NH_3 groups have short H-bonds (1.92 Å and 2.05 Å) to the carbonyl oxygen (of chain b or chain a, respectively) of the coordinated DHPA molecules. One of the *cis*-NH_3 groups has a single H-bond (distance = 2.23 Å) to the phosphate oxygen atom of the coordinated DHPA, whilst the other has a longer H-bond to phosphate oxygen (distance = 2.84 Å) and an additional H-bond (distance = 2.02 Å) to the carbonyl oxygen of chain b of the coordinated DHPA.

<Insert Figure 3 and Figure 4 here>

In the case where there is no interaction between the two {PtN_3Y} moieties, the H-bonding interactions between the Pt-a(m)mine units and the coordinated DHPA molecules are expected to be similar to that of the monofunctional adduct (coincident peaks C_m/C_b in Fig. 1). The DFT model of the bifunctional adduct (1,1/*c,c*-BF-2) shown in Fig. 2(d) (and Fig. 4(c and d)), is largely consistent with the NMR results, except there are short H-bonds between aliphatic chain carbonyl oxygen atoms and both *trans*-NH_3 groups. Whilst there are no similar H-bonds in the 1,1/*c,c*-MF-2 model (Fig. 2(b)), they are found in the 1,1/*c,c*-MF-1 model (see above) and thus it is reasonable to assume that NMR peaks for the different adducts will be strongly overlapped.

Kinetics

The time dependence of the concentrations of species in the reaction (1:5 ^{15}N-**1**:DHPA) are shown in Fig. 5. Notable differences between the reaction of ^{15}N-**1** with 1,1/*t,t* are the much greater proportion of DHPA adduct formed in the present case and the slower attainment of equilibrium.[10] For ^{15}N-**1** only 9% of the total Pt remained coordinated to chloride at equilibrium (120 h) compared to 35% for 1,1/*t,t* after 35 h.[10]

To allow comparison with the reactions with 1,1/*t,t*, the same kinetic model (Scheme 1) that was previously reported[10] was used for the reaction with ^{15}N-**1**, with the concentrations of species based on the $^1H,^{15}N$ peaks in the *cis*-NH_3 region, so that species C is derived from both monofunctional and bifunctional adducts. The curves are computer best fits and the rate constants are tabulated in Table 2.

<Insert Scheme 1 here>
<Insert Figure 5 and Table 2 here>

We have used previously [$^1H,^{15}N$] HSQC NMR to investigate also the aquation of ^{15}N-**1** and 1,1/*t,t* in the presence of phosphate, under similar conditions (pH 5.3-5.9, 298K) to those used here in the reaction with DHPA.[6] The rate and equilibrium constants for these reactions, obtained from the simplified kinetic model (analogous to that in Scheme 1) are listed also in Table 2.

For reactions in phosphate, equilibrium conditions for 1,1/*t,t* are established far more rapidly than for cisplatin,[11] due to the higher anation rate constant keeping the equilibrium more to the chlorido form. An important feature of the reaction of 1,1/*t,t* in phosphate is the high value for the rate constant for the reverse reaction (k_{-L}); comparison of pK_1 and pK_L in Table 2 demonstrate the clear preference for chloride over phosphate. For 1,1/*t,t* the equilibrium in phosphate was attained after 12 h and strongly favoured the dichlorido species. For 1,1/*c,c*, equilibrium conditions in the presence of phosphate are reached much more slowly (> 80 h) than for 1,1/*t,t* due to the slower (6-fold) aqua displacement of the bound phosphate – resulting in a greater proportion of phosphate-bound species at equilibrium.[6]

Comparison of the rate constants (Table 2) shows that the rate constant for the first step of DHPA binding (k_L) is slightly lower (1.6 fold) for the *cis*- compared to the *trans*-isomer, whereas the rate constants for the reverse reaction is 4-fold lower for 1,1/*c,c*. For 1,1/t,t the rate constant for the first step of DHPA binding (k_L) is about 8 times higher than that for phosphate binding, but the rate constants for the reverse reactions are quite similar so that equilibrium conditions are attained more slowly. On the hand for 1,1/*c,c* , k_L is 6-fold higher for DHPA compared to phosphate, whist k_{-L} is 5-fold lower, so that overall equilibrium conditions are attained after a similar time (120 h). The reduced lability of the bound phosphate was attributed to the ability to form a macrochelate-phosphate bridged species.[6] Whilst a comparable species is not

observed in the present case the formation of mono- (1,1/*c,c*-MF-1) and bifunctional (1,1/*c,c*-BF-1) DHPA adducts in which there is an interaction between the two {PtN_3Y} groups (a feature only accessible for the *cis* geometric isomer) provides an explanation for the slower release of the bound DHPA molecules.

Conclusions

These results confirm the relevance of phospholipid interactions for a full description of the biology of platinum antitumour agents. There are distinct differences between the pair of geometric 1,1/*t,t* and 1,1/*c,c* isomers, with equilibrium conditions being reached much more slowly for the latter. Further, the comparison of the forward and reverse rate constants show that in the 1,1/*c,c* case there is a much greater proportion of DHPA-bound species at equilibrium. These geometric differences may also extrapolate to the mononuclear *cis* and *trans*-[$PtCl_2(NH_3)_2$] pair. While significant work has been done on DNA interactions to explain the lack of meaningful anticancer activity of the *trans* isomer, much less comparative information is available for the mononuclear pair with other relevant biomolecules such as phospholipids. Since the 1,1/*c,c* compound contains the same geometrical configuration as cisplatin – the presence of *cis*-{$Pt(NH_3)_2$} coordination spheres - the interactions observed here may be extrapolated to possible weak interactions of cisplatin itself. As we have observed, the cellular localization and concentration of biomolecules such as phospholipids or heparan sulfate, which are predominantly oxygen-donors, does not preclude loose association of small molecules such as cisplatin, and these cellular entities may better describe the immediate fate of cisplatin, rather than existing as simple aquated cations.

Unlike the mononuclear pair, both the 1,1/*t,t* and 1,1/*c,c* isomers are antitumour active. Cellular accumulation in the murine leukaemia L1210/0 observes the relative order 1,0,1/*t,t,t* > 1,1/c,*c* > cisplatin > 1,1/*t,t*, but with overall similar levels of accumulation. In the resistant cell line L1210/DDP accumulation of cisplatin and the two dinuclear complexes, is diminished whereas accumulation of Triplatin is essentially equivalent.[12] Previous studies also indicated that the 1,1/*c,c* isomer was less collaterally sensitive to cisplatin (that is the 1,1/*c,c* was less able to overcome cisplatin resistance).[12] Phospholipids are one of the major components of cell membranes and diminished accumulation of the dinuclear compounds may reflect their sequestering by membrane components such as phospholipids. In this respect, the previously observed "non-covalent" interactions observed with the 4+ Triplatin compared to the dinuclear pair may contribute to the enhanced internalization and greater ability to overcome cisplatin resistance, given that reduced cellular accumulation is a significant contributor to cisplatin resistance.

The amphipathic nature of PPCs where lipophilic diamine chains link hydrophilic Pt-am(m)ine coordination spheres is remarkably complementary for strong interaction with the amphiphilic phospholipids. This complementarity is not available to the smaller cisplatin, which may engage in weak covalent phosphate interactions, but has no intrinsic lipophilic component. The effectiveness of the incorporation of cisplatin, carboplatin and oxaliplatin into liposomes to enhance biodistribution and lower toxicity may be diminished in the absence of this complementarity, which may affect release rates of the drug.[13-15] In general, the ability to systematically target membrane biomolecules suggest approaches to drug design that can play a significant role in dictating the *overall* biology of platinum drugs and have *functional* consequences contributing to the overall cytotoxic profile of platinum agents.

Experimental

Materials

1,2-dihexanoyl-*sn*-glycero-3-phosphate (monosodium salt) (DHPA) was purchased from Avanti. The nitrate salt of ^{15}N labelled [{*cis*-$PtCl(NH_3)_2\}_2(\mu$-$NH_2(CH_2)_6NH_2)]^{2+}$ (1,1/c,c; ^{15}N-**1**) was prepared from *cis*-[$PtCl_2(^{15}NH_3)_2$] and $AgNO_3$ using procedures similar to those previously published.[16]

Sample Preparation

15 mM stock solution of phospholipid was prepared by dissolving DHPA (10 mg, 0.026 mmol) in double distilled H_2O (1.71 mL) and adjustment of the pH to 5.4 using 0.1-1 M NaOH or $HClO_4$.

Reaction of 1,1/*c,c* (^{15}N-1) with DHPA (1:5 ratio)

Freshly prepared solution of ^{15}N-labelled 1,1/*c,c* (^{15}N-**1**) (0.35 mg, 0.45 μmol) in H_2O (30 μL) was combined with 15 mM DHPA stock solution (160 μL), 200 mM $NaClO_4$ (240 μl), H_2O (54 μL), D_2O (24 μl) and 10 mM TSP (2 μL) to give a total volume of 480 μl and final concentrations of 1,1/*c,c* (1 mM) and DHPA (5 mM) in 100 mM $NaClO_4$. The starting pH was 5.6.

NMR Spectroscopy

The NMR spectra were recorded on a Bruker 600 MHz spectrometer (^1H, 600.1 MHz; ^{15}N, 60.8 MHz; ^{31}P, 242.9; ^{195}Pt, 129.0 MHz) fitted with a pulsed field gradient module and 5 mm triple resonance probehead. The ^1H NMR chemical shifts are internally referenced to TSP (sodium 3-trimethylsilyl-[D4]-propionate) and the ^{15}N chemical shifts externally referenced to $^{15}NH_4Cl$ (1.0 M in 1.0 M HCl in 5% D_2O in H_2O). The ^1H spectra were acquired with water suppression using the watergate 3-9-19 pulse sequence.[17, 18] The two-dimensional [^1H,^{15}N] heteronuclear single-quantum coherence (HSQC) NMR spectra optimized for $^1J(^{15}N,^1H)$ = 72 Hz were recorded using standard Bruker phase sensitive HSQC pulse sequence.[19] The ^{15}N signals were decoupled by irradiating with the GARP-1 sequence at field strength of 6.9 kHz during the acquisition time. Typically for 1D ^1H spectra, 32 scans and 32 K points were acquired using a spectral width of 12 kHz and a relaxation delay of 2.5 s. For kinetics studies involving [^1H, ^{15}N] HSQC NMR spectra, 4 transients were collected for 96 increments of t_1 (allowing spectra to be recorded on a suitable timescale for the observed reaction), with an acquisition time of 0.069 s, spectral widths of 6 kHz in f_2 (^1H) and 5.5 kHz in f_1 (^{15}N). 2D spectra were completed in 14 minutes. The 2D spectra were processed using zero-filling up to the next power of 2 in both f_2 and f_1 dimensions.

NMR spectra were recorded at 298 K, and the sample was maintained at this temperature when not immersed in the NMR probe. NMR sample (including buffers, acids, etc.) was prepared so that there was a 5% D_2O / 95% H_2O concentration (for deuterium lock but with minimal loss of signal as a result of deuterium exchange). The pH of the solution was measured on a Shindengen pH Boy-P2 (su19A) pH meter and calibrated against pH buffers of pH 6.9 and 4.0. The volume of 5.0 μL of the solution was placed on the electrode surface and the pH recorded. These aliquots were not returned to the bulk solution (as the electrode leaches Cl^-). Adjustments in pH were made using 0.1 M and 1.0 M $HClO_4$ in 5% D_2O in H_2O, or 0.1 M and 1.0 M NaOH in 5% D_2O in H_2O.

Data Analysis

The kinetic analysis of the reactions was undertaken by measuring peak volumes in the *cis*-NH_3 region of the [^{1}H,^{15}N] HSQC NMR spectra using the Bruker XWINNMR software package and calculating the relative concentrations of the various species at each time point, in the same manner as described previously for the reactions of 1,1/*t,t* and 1,1/*c,c* with phosphate.[6] Peak volumes were determined using an identical vertical scale and threshold value. In order to simplify the system, we used a simplified model in which the species derived from ^{15}N-**1** are treated as mononuclear [*cis*-$Pt(NH_3)_2(NH_2(CH_2)_6NH_2)Y]^{n+}$. In this case the total volume for each peak accounted for the total concentration of Pt-Cl (A), Pt-OH_2 (B) or ligated (DHPA adducts C or D) species (see Scheme 2). The peak volumes were normalized and the concentration of each species was determined for each spectrum based on the initial concentration of the parent complex. The data were then subjected to kinetic analysis. The appropriate differential equations were integrated numerically and rate constants determined by a non-linear optimization procedure using the program SCIENTIST (Version 2.01, Micromath Inc.), as we have described previously.[6] The errors quoted represent one standard deviation. The kinetic models for all reactions are depicted and the rate and equilibrium constants are defined in Scheme 1.

DFT Calculations

All DFT computations were performed using the Gaussian 16 suite of programs[20] either on the Griffith University's HPC cluster, Gowonda, or on clusters at the National Computing Infrastructure (NCI). The hybrid version of the parameter-free PBE functional, PBE0, which demonstrated excellent performance for geometry optimization of transition metal complexes, was used for these computations. Full geometry optimizations without any constraints were performed with 6-31G(2d,2p) for C, H, N, P, O and Hay and Wadt effective core potential (LanL2DZ) basis sets for Pt, with diffuse functions only on oxygen. All systems were solvated using the IEFPCM solvation model with water as solvent. NMR data suggested that 1,1/*c,c* forms two mono and two bifunctional adducts with DHPA. The starting structure for the first mono adduct (1,1/*c,c*-MF-1) was analogous to the previously reported aquaphosphato model of 1,1/*c,c*,[6] whilst the starting structure for the second (1,1/*c,c*-MF-2) was constructed in a similar manner to that of the previously reported 1,1/*t,t* monofunctional adduct.[10] For the first bifunctional adduct (1,1/*c,c*-BF-1), DHPA fragments at both ends in the starting structure were constructed in a *cis* orientation to each other. The starting structure for the second bifunctional adduct (1,1/*c,c*-BF-2) was constructed by introducing a DHPA molecule at the {PtN_3Cl} end of the DFT optimized structure of 1,1/*c,c*-MF-1, in a similar orientation to that of the coordinated DHPA molecule. All the systems were pre-optimized using the semi-empirical method, PM6, MOPAC[21] and the resulting geometry was then used as the input for DFT calculations.

Conflicts of interest

There are no conflicts to declare.

Acknowledgements

The work was supported by grants from the Australian Research Council (DP1095383 and DP150100308) to SJBP and NPF and NIH (RO1CA78754) to NPF. We thank Dr. Yun Qu and Dr. Donald Thomas for assistance with NMR spectra. The DFT study in this work was undertaken with the assistance of resources and services from the National Computational Infrastructure (NCI), which is supported by the Australian Government. We also gratefully acknowledge the support of the Griffith University eResearch Services Team and the use of the High Performance Computing Cluster "Gowonda" to complete this research.

References

1 F. Basolo and R. G. Pearson, *Mechanisms of Inorganic Reactions*, John Wiley and Son, New York, 1967.
2 S. J. Berners-Price, T. A. Frenkiel, U. Frey, J. D. Ranford and P. J. Sadler, *J. Chem. Soc. Chem. Commun.*, 1992, 789-791.
3 S. J. Berners-Price, L. Ronconi and P. J. Sadler, *Prog. Nucl. Magn. Reson. Spectr.*, 2006, **49**, 65-98.
4 M. S. Davies, J. W. Cox, S. J. Berners-Price, W. Barklage, Y. Qu and N. Farrell, *Inorg. Chem.*, 2000, **39**, 1710-1715.
5 M. S. Davies, D. S. Thomas, A. Hegmans, S. J. Berners-Price and N. Farrell, *Inorg. Chem.*, 2002, **41**, 1101-1109.
6 J. Zhang, D. S. Thomas, M. S. Davies, S. J. Berners-Price and N. Farrell, *J. Biol. Inorg. Chem.*, 2005, **10**, 652-666.
7 R. A. Ruhayel, B. Corry, C. Braun, D. S. Thomas, S. J. Berners-Price and N. P. Farrell, *Inorg. Chem.*, 2010, **49**, 10815-10819.
8 H. Silva, F. Frézard, E. J. Peterson, P. Kabolizadeh, J. J. Ryan and N. P. Farrell, *Mol. Pharm.*, 2012, **9**, 1795-1802.
9 A. K. Gorle, P. Rajaratnam, C.-W. Chang, M. von Itzstein, S. J. Berners-Price and N. P. Farrell, *Inorg. Chem.*, 2019, in press, 10.1021/acs.inorgchem.1028b03035.
10 A. K. Gorle, J. Zhang, Q. Liu, S. J. Berners-Price and N. P. Farrell, *Chem. Eur. J.*, 2018, **24**, 4643-4652.
11 M. S. Davies, S. J. Berners-Price and T. W. Hambley, *Inorg. Chem.*, 2000, **39**, 5603-5613.
12 J. D. Roberts, J. Peroutka and N. P. Farrell, *J. Inorg. Biochem.*, 1999, **77**, 51-57.
13 I. H. L. Hamelers, E. van Loenen, R. W. H. M. Staffhorst, B. de Kruijff and A. I. P. M. de Kroon, *Mol. Cancer Ther.*, 2006, **5**, 2007-2012.
14 S. H. Alavizadeh, A. Badiee, S. Golmohammadzadeh and M. R. Jaafari, *Int. J. Pharm.*, 2014, **473**, 326-333.
15 H. M. Kieler-Ferguson, D. Chan, J. Sockolosky, L. Finney, E. Maxey, S. Vogt and F. C. Szoka, *Eur. J. Pharm. Sci.*, 2017, **103**, 85-93.
16 N. Farrell, T. G. Appleton, Y. Qu, J. D. Roberts, A. P. S. Fontes, K. A. Skov, P. Wu and Y. Zou, *Biochemistry*, 1995, **34**, 15480-15486.
17 V. Sklenar, M. Piotto, R. Leppik and V. Saudek, *J. Magn. Reson. A*, 1993, **102**, 241-245.
18 M. Piotto, V. Saudek and V. Sklenar, *J. Biomol. NMR*, 1992, **2**, 661-666.
19 A. G. Palmer, III, J. Cavanagh, P. E. Wright and M. Rance, *J. Magn. Reson.*, 1991, **93**, 151-170.
20 M. J. Frisch, G. W. Trucks, H. B. Schlegel, G. E. Scuseria, M. A. Robb, J. R. Chesseman, G. Scalmani, V. Barone, B. Mennucci, G. E. Peterson and H. Nakatsuji, in *Gaussian 16*, 2016.
21 J. J. Stewart, *Stewart Computational Chemistry*, 2012.

a

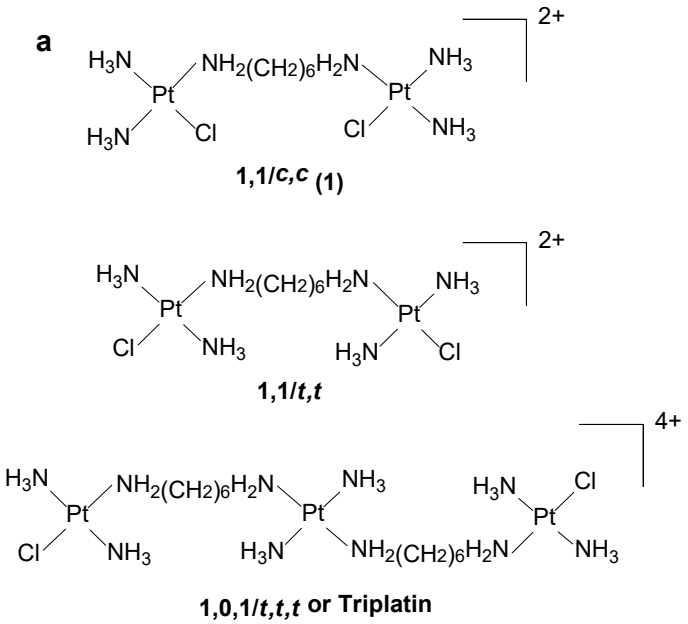

b

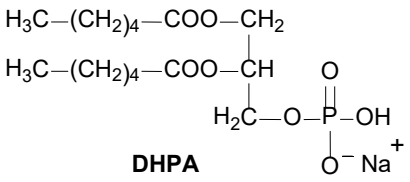

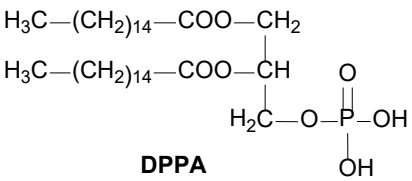

Chart 1 Structures of the platinum complexes and phospholipids discussed in this work.

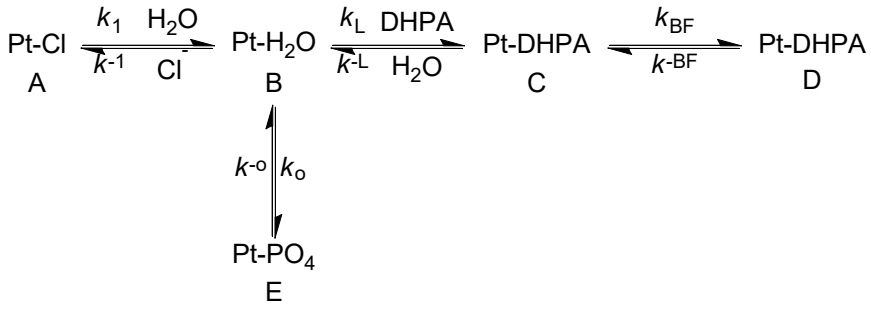

Scheme 1 Pathways for the reaction of 1,1/c,c (**1**) with DHPA, from analysis of the time dependence of peaks in the [^{1}H,^{15}N] HSQC NMR spectra (Fig. 1). A simplified kinetic model was used for the equivalent {PtN_3Y} end groups in different species that were indistinguishable. The species "D" corresponds only to bifunctional adducts, whereas species "C" is derived from both monofuctional and bifunctional adducts (see text). "E" corresponds to a minor product from the reaction of ^{15}N-**1** with a minor hydrolysis product of DHPA[10] and accounts for 9% of the total species at equilibrium (Fig. 5). The derived rate constants are shown in Table 2.

Table 1. ^{1}H and ^{15}N chemical shifts for species observed during the reaction of ^{15}N-labelled 1,1/*c,c* (**1**) with DHPA in 100 mM $NaClO_4$ at 298 K.[a]

Compound	Species	*cis*-NH_3		Pt-NH_2		*trans*-NH_3	
		δ ^{1}H	δ ^{15}N	δ ^{1}H	δ ^{15}N	δ ^{1}H	δ ^{15}N
1,1/*c,c*	Pt-Cl(A)[b]	3.76	−66.0	4.49	−44.2	4.29	−68.8
	Pt-H_2O(B)	3.92	−63.9	4.61	−42.1	4.22	−84.2
	Pt-DHPA (C_m/C_b)[b]	3.86	−65.3	4.56	−43.5	4.21	−83.6
	Pt-DHPA(D)	3.90	−65.3	4.65	−42.8	4.26	−84.0
	Pt-PO_4(E)[c]	3.86	−62.5	4.64	−41.5	4.17	−86.4

[a] ^{1}H referenced to TSP (sodium 3-trimethylsilyl-[D4]-propionate); ^{15}N referenced to $^{15}NH_4Cl$ (external). [b] For one conformer of the mono DHPA adduct the *trans*-NH_3 and Pt-NH_2 peaks of the {PtN_3Cl} unbound end are distinguishable from those of the parent chlorido complex at δ ^{1}H/^{15}N = 4.32/−68.2 and 4.61/−42.8, respectively (see Fig. 1(b) and (c), peaks labelled $C_{m'}$). [c] Product from the reaction of ^{15}N-**1** with a minor hydrolysis product of DHPA, which has ^{1}H,^{15}N chemical shifts similar to that of the {$PtON_3$} unit of the chlorophosphato species formed on reaction of ^{15}N-**1** with phosphate at a similar pH;[6] analogous minor products were observed in the reactions of 1,1/*t,t* and 1,0,1/*t,t,t* with the same DHPA sample.[10]

Table 2. Rate and equilibrium constants for the reaction of **1** with DHPA in 100 mM $NaClO_4$ at 298 K, pH 5.6 in comparison to phosphate and DHPA reactions of 1,1/*t,t* and 1,0,1/*t,t,t*.[a]

	1,1/*c,c* (**1**)		1,1/*t,t*	
Parameter	DHPA	phosphate[b]	DHPA[c]	phosphate[b]
k_1(10^{-5}·s^{-1})	2.07 ± 0.05	2.18 ± 0.03	2.64 ± 0.10	2.49 ± 0.04
k_{-1} (M^{-1}·s^{-1})	0.13 ± 0.01	0.145 ± 0.005	0.197 ± 0.020	0.40 ± 0.01
k_L (M^{-1}·s^{-1})	0.045 ± 0.002	0.0071 ± 0.0001	0.075 ± 0.010	0.0086 ± 0.0002
k_{-L}(10^{-5}·s^{-1})	0.15 ± 0.02	0.70 ± 0.02	5.68 ± 1.03	3.9 ± 0.1
k_o (M^{-1}·s^{-1})	0.0060 ± 0.0005		0.0035 ± 0.0009	
k_{-o} (10^{-5}·s^{-1})	0.23 ± 0.04		0.95 ± 0.35	
k_{BF} (10^{-5}·s^{-1})	2.48 ± 0.45		3.42 ± 0.32	
k_{-BF}(10^{-5}·s^{-1})	8.41 ± 1.58		2.35 ± 0.26	
pK_1	3.81 ± 0.05	3.82 ± 0.02	3.87 ± 0.06	4.21 ± 0.02
pK_L	−4.49 ± 0.07	−3.01 ± 0.02	−3.12 ± 0.14	−2.34 ± 0.02
pK_o	−3.43 ± 0.11		−2.56 ± 0.32	
pK_{BF}	0.53 ± 0.17		−0.16 ± 0.09	

[a] The rate constants for reaction with DHPA were derived from the kinetic model in Scheme 1. [b] Values for phosphate taken from ref.[6] for the related simplified kinetic model. [c] Values for the DHPA binding of 1,1/*t,t* are taken from ref.[10].

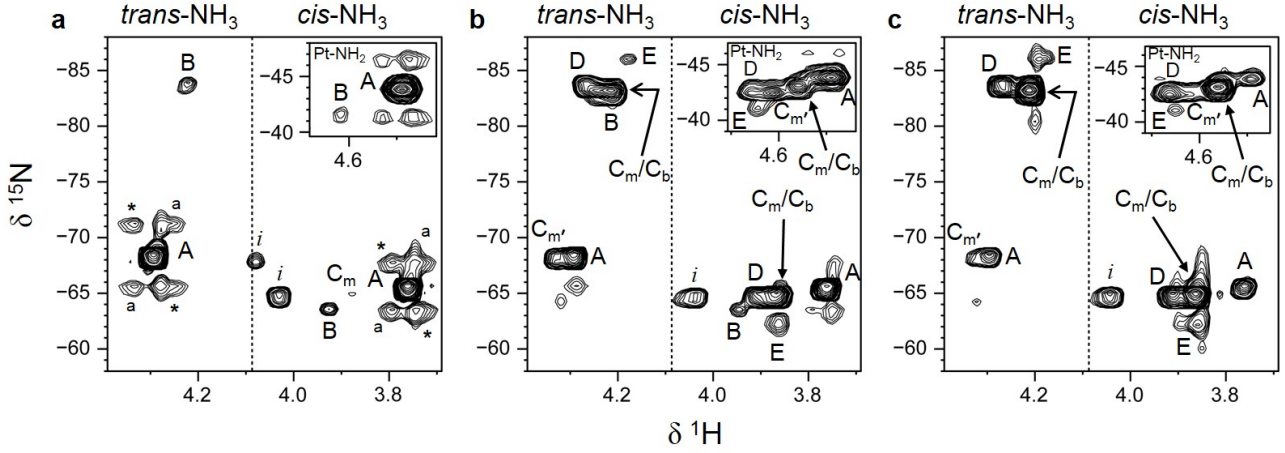

Figure 1. 2D [^{1}H,^{15}N] HSQC NMR (600 MHz) spectra at 298K of ^{15}N-**1** (1 mM) with DHPA (5 mM) in 100 mM $NaClO_4$ (a) after 36 min, (b) 17.4 h and (c) 117 h after mixing. The Pt-NH_2 region is shown as an inset.

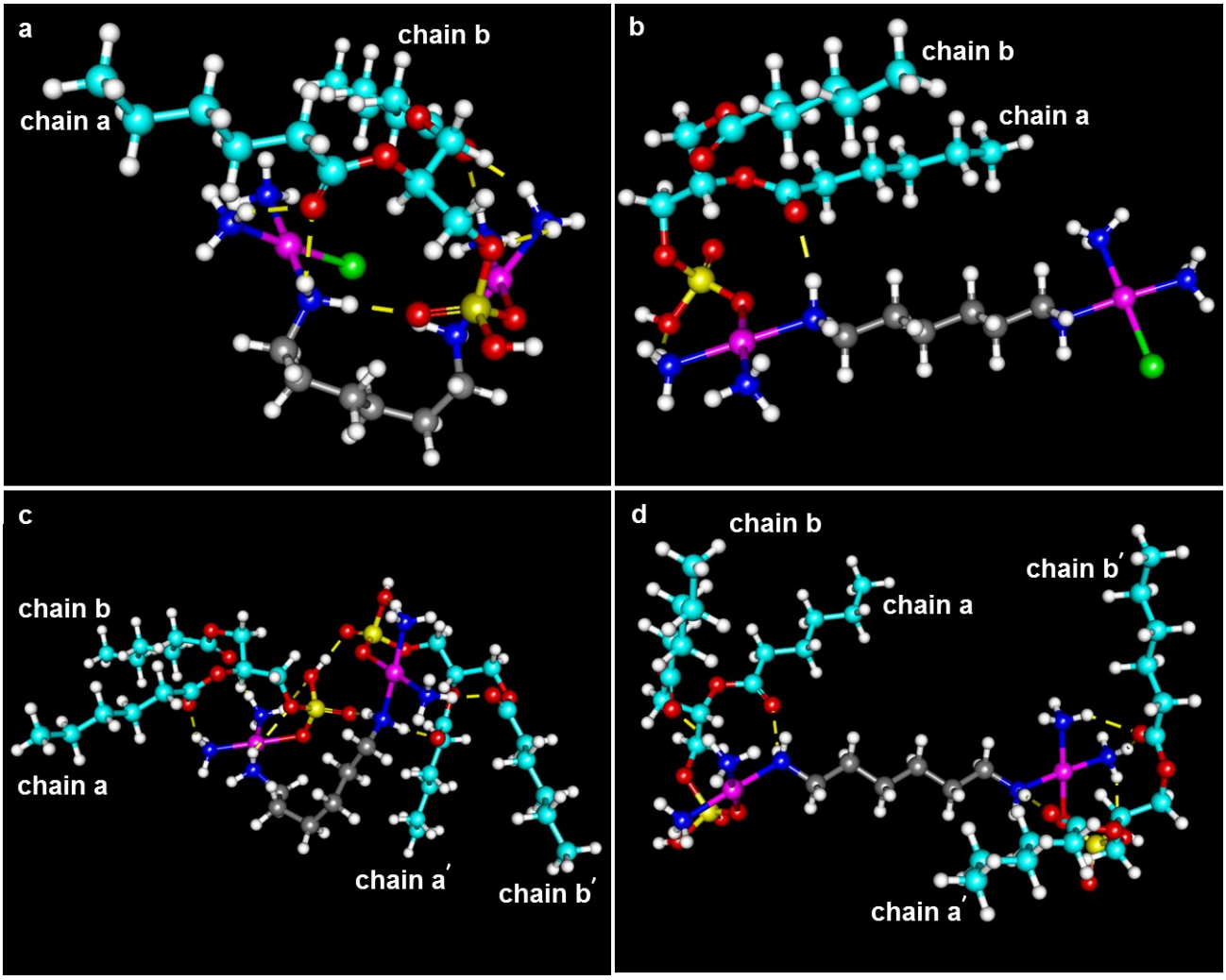

Figure 2. DFT optimized models of the DHPA bound adducts of 1,1/*c,c* (**1**). Two different orientations of the $(CH_2)_6$ linker lead to different conformers of the monofunctional (1,1/c,c-MF-1 (a) and (1,1/c,c-MF-2 (b)) and bifunctional (1,1/c,c-BF-1 (c) and 1,1/c,c-BF-2 (d)) adducts. In (a) and (c) there is an interaction between the two {PtN_3Y} coordination spheres. The models are largely consistent with the ^{1}H,^{15}N peaks observed in the [^{1}H,^{15}N] HSQC NMR spectra (Fig. 1). Expansions showing the details of the H-bonding interactions are shown in Fig. 3 and Fig. 4.

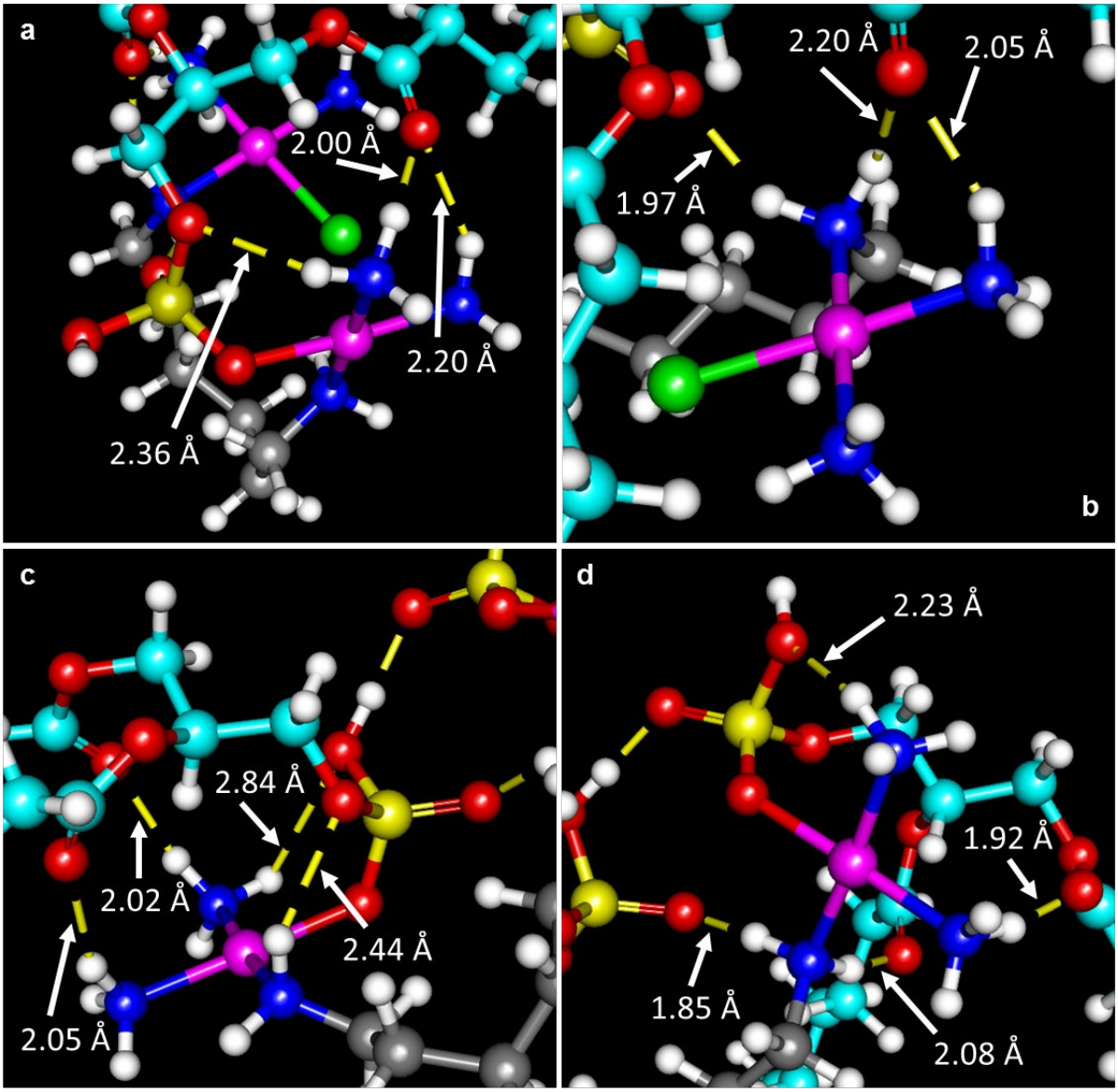

Figure 3. Hydrogen bonding interactions in the DFT optimized DHPA bound adducts of 1,1/*c,c* (**1**) in which there is an interaction between the two {PtN_3Y} coordination spheres (Fig. 2). (a) and (b) the monofunctional adduct (1,1/*c,c*-MF-1; see Fig. 2(a)); (c) and (d) the bifunctional adduct (1,1/*c,c*-BF-1; see Fig. 2(c)).

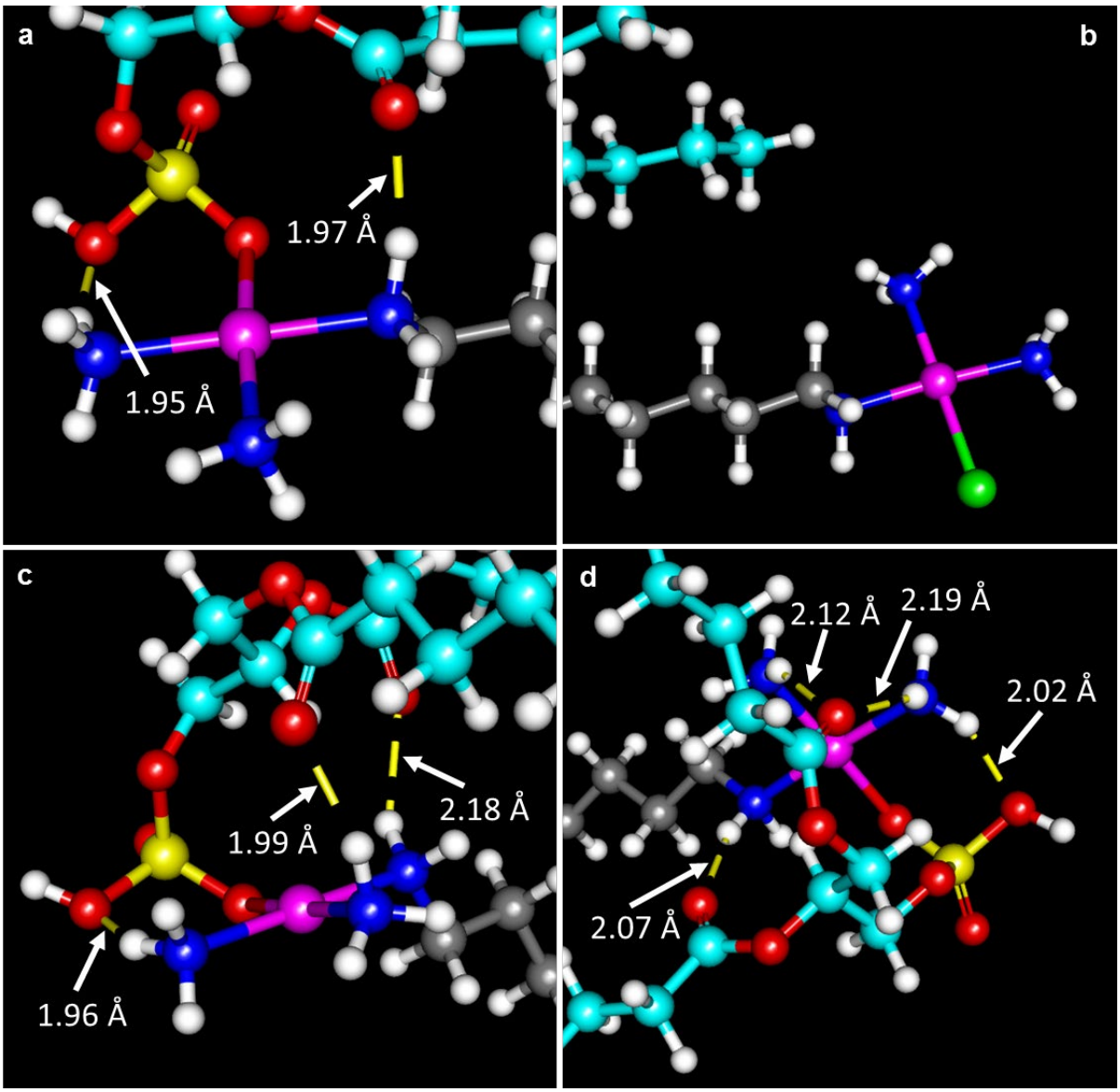

Figure 4. Hydrogen bonding interactions in the DFT optimized DHPA bound adducts of 1,1/*c,c* (**1**) in which there is no interaction between the two {PtN_3Y} coordination spheres (Fig. 2). (a) and (b) the monofunctional adduct (1,1/*c,c*-MF-2; see Fig. 2(b)); (c) and (d) the bifunctional adduct (1,1/*c,c*-BF-2; see Fig. 2(d)).

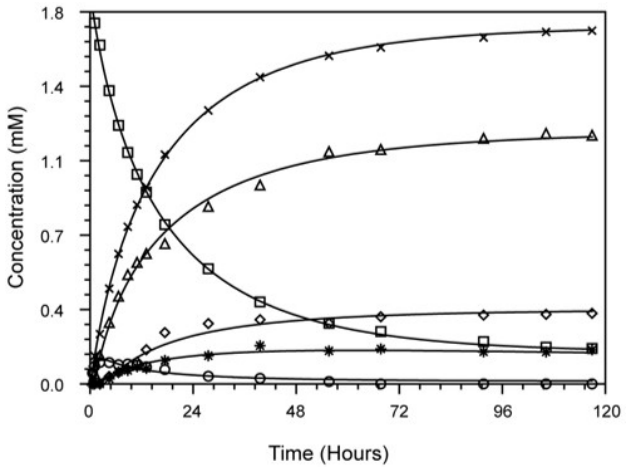

Figure 5. Plot of the time dependence of species observed in the reaction of ^{15}N-**1** (1,1/*c,c*) with DHPA (1: 5 ratio) in 100 mM $NaClO_4$. The curves are computer best fits to the model shown in Scheme 1. The concentrations are based on the ^{1}H,^{15}N peaks in the *cis*-NH_3 region (Fig. 1) and refer to the {PtN_3Y} end groups so that the initial concentration of **A** (Pt-Cl) is twice that of ^{15}N-**1.** The rate constants are provided in Table 2. Key: **A** *open squares*; **B** *open circles*; **C** *open triangles*; **D** *open diamonds*; **E** *asterisk*; released chloride **x**.